ARTICLES
https://doi.org/10.1038/s41567-022-01520-3

nature physics

OPEN

Tumour irradiation in mice with a laser-accelerated proton beam

Florian Kroll[1]✉, Florian-Emanuel Brack[1,2], Constantin Bernert[1,2], Stefan Bock[1], Elisabeth Bodenstein[3], Kerstin Brüchner[1,2,3], Thomas E. Cowan[1,2], Lennart Gaus[1,2], René Gebhardt[1], Uwe Helbig[1], Leonhard Karsch[1,3], Thomas Kluge[1], Stephan Kraft[1], Mechthild Krause[1,3,4,5,6,7], Elisabeth Lessmann[1], Umar Masood[1], Sebastian Meister[1], Josefine Metzkes-Ng[1], Alexej Nossula[1], Jörg Pawelke[1,3], Jens Pietzsch[1,2], Thomas Püschel[1], Marvin Reimold[1,2], Martin Rehwald[1,2], Christian Richter[1,3,4,5,6], Hans-Peter Schlenvoigt[1], Ulrich Schramm[1,2], Marvin E. P. Umlandt[1,2], Tim Ziegler[1,2], Karl Zeil[1] and Elke Beyreuther[1,3]

Recent oncological studies identified beneficial properties of radiation applied at ultrahigh dose rates, several orders of magnitude higher than the clinical standard of the order of Gy min^{-1}. Sources capable of providing these ultrahigh dose rates are under investigation. Here we show that a stable, compact laser-driven proton source with energies greater than 60 MeV enables radiobiological in vivo studies. We performed a pilot irradiation study on human tumours in a mouse model, showing the concerted preparation of mice and laser accelerator, dose-controlled, tumour-conform irradiation using a laser-driven as well as a clinical reference proton source, and the radiobiological evaluation of irradiated and unirradiated mice for radiation-induced tumour growth delay. The prescribed homogeneous dose of 4 Gy was precisely delivered at the laser-driven source. The results demonstrate a complete laser-driven proton research platform for diverse user-specific small animal models, able to deliver tunable single-shot doses up to around 20 Gy to millimetre-scale volumes on nanosecond timescales, equivalent to around 10^9 Gy s^{-1}, spatially homogenized and tailored to the sample. The platform provides a unique infrastructure for translational research with protons at ultrahigh dose rates.

Since the beginning of external beam radiotherapy (RT), accelerator research and development has constantly advanced RT technology for the treatment of cancer patients[1]. Here translational research streamlines the transition to specialized radiation sources and dose application systems for improved patient care[2]. Recently, the biological effect termed FLASH has been discussed as a promising candidate for the next advancement in cancer RT[3–5]. As per the current knowledge in this rapidly evolving field, this effect is triggered through a fast dose delivery (<100 ms) at mean dose rates ($\gtrsim$40 Gy s^{-1}) beyond the clinically administered rates (approximately Gy min^{-1})[6–8]. By simultaneously offering an unaltered tumour response and reduced normal tissue toxicity, FLASH promises dose escalation by shifted normal tissue dose constraints and the rapid dose applications allow the freezing of organ motion during treatment. Both qualities suggest an enhanced quality of life of radiotherapy patients[6,9]. Yet, the step to FLASH RT for curative treatment requires detailed radiobiological in vivo studies on normal and tumour tissue response with respect to temporal dose delivery parameters, namely, dose per bunch, bunch repetition frequency, bunch dose rate, mean dose rate, fractionation and total irradiation time[3,9–11]. Technology-wise, these investigations depend on research accelerator infrastructure for small animal studies, providing flexible dose and dose rate delivery schemes[6,9,11], ideally capable of scanning dose application times from femtoseconds to minutes as relevant for the cascade of physical, chemical and biological events in the interaction of ionizing radiation with tissue[5]. Other than electrons and X-rays, indications for beneficial dose rate effects for proton RT, the most advanced RT modality, remain inconclusive[12] as the portfolio of accelerators capable of delivering ultrahigh mean and bunch dose rates is limited[11,13–16].

Here we investigate how proton sources based on laser–plasma acceleration (LPA) can fill this gap. Proton LPA relies on the interaction of an intense (>10^{18} W cm^{-2}) femtosecond to picosecond short laser pulse with a solid target of nanometre-to-micrometre thickness. The laser turns the target into a plasma capable of supporting electric fields of approximately teravolts per metre. These accelerate intense proton bunches of approximate picosecond duration to multi-10-MeV kinetic energies on a micrometre scale at the repetition rate of the laser ($\lesssim$1 Hz)[17]. A single ultrashort LPA proton bunch contains up to 10^{12} protons with a broad angular distribution and exponentially decaying energy spectrum with a cut-off towards higher kinetic energies (Fig. 1b). This unique combination of temporal, spatial and

[1]Helmholtz-Zentrum Dresden-Rossendorf, Dresden, Germany. [2]Technische Universität Dresden, Dresden, Germany. [3]OncoRay—National Center for Radiation Research in Oncology, Faculty of Medicine and University Hospital Carl Gustav Carus, TU Dresden, Helmholtz-Zentrum Dresden-Rossendorf, Dresden, Germany. [4]German Cancer Consortium (DKTK), Partner Site Dresden, Dresden, Germany. [5]National Center for Tumor Diseases (NCT), Partner Site Dresden: German Cancer Research Center (DKFZ), Faculty of Medicine and University Hospital Carl Gustav Carus, Technische Universität Dresden, Germany, Helmholtz Association/Helmholtz-Zentrum Dresden-Rossendorf (HZDR), Dresden, Germany. [6]Department of Radiotherapy and Radiation Oncology, Faculty of Medicine and University Hospital Carl Gustav Carus, Technische Universität Dresden, Dresden, Germany. [7]Department for Radiotherapy and Radiooncology, University Hospital Carl Gustav Carus, Technische Universität Dresden, Dresden, Germany.
✉e-mail: florian.kroll@hzdr.de

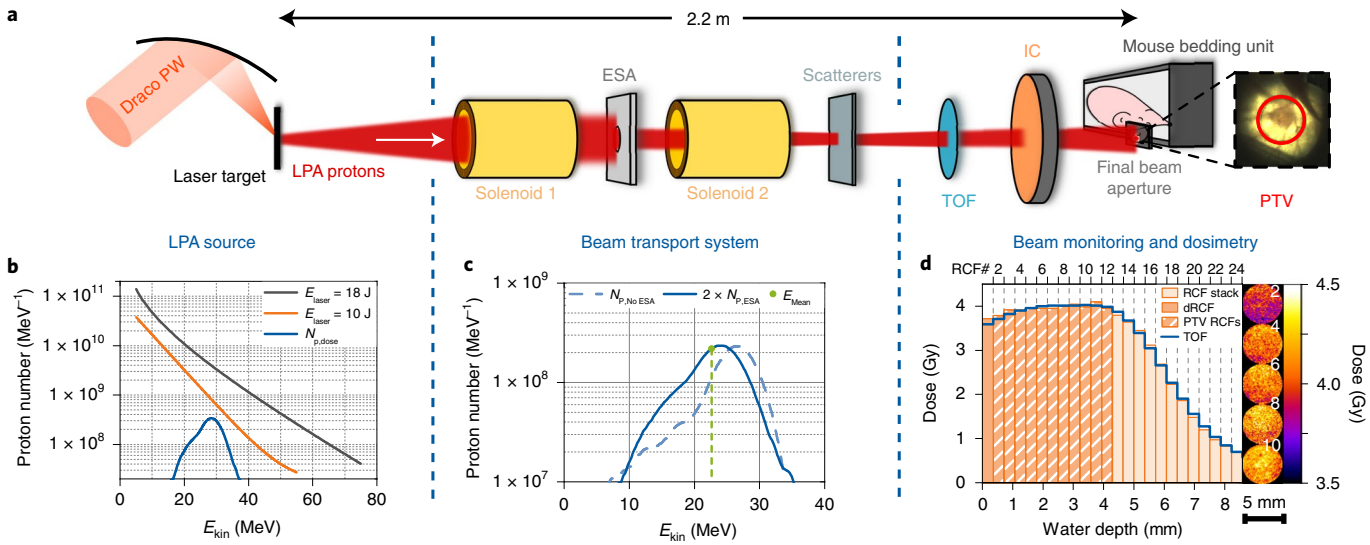

Fig. 1 | Overview of the model-conform dose delivery at Draco PW. a, The Draco PW laser, impinging on the laser target, drives a broadband LPA proton source. A selected spectral part of the protons is transported using a pulsed two-solenoid beamline. The ESA is inserted for spectral shaping and scatterers for lateral homogenization. The protons traverse the beam monitors and dosimeters installed downstream in air, before delivering the dose to the PTV behind the final beam aperture of the mouse bedding unit. **b**, Kinetic energy (E_{kin}) proton-source spectra at the Draco PW laser measured by stacked RCFs for two laser energies (E_{laser}) on target (Methods). $N_{p,dose}$ represents the fraction of the orange-source spectrum required for dose delivery. **c**, TOF-measured kinetic energy (E_{kin}) of the proton-source spectra at the PTV position with and without ESA of 15 mm ($2\times N_{P,ESA}$ (solid blue line) and $N_{P,No\ ESA}$ (dashed blue line)). The green data represent the mean proton bunch energy E_{Mean}. **d**, Integral depth–dose distribution measured via the RCF stack compared with the TOF prediction (blue). The dose in the dRCF is highlighted in dark orange and the dose in the PTV is shown by the dashed line (PTV RCFs). Pseudo-colour images show the lateral dose distributions at selected RCF stack layers within the PTV.

spectral bunch properties makes proton LPA sources inherently suitable for ultrahigh-dose-rate radiobiology studies, motivating different user facilities[18,19], as well as allowing for single-shot dose escalation. Related research with LPA protons has so far been limited to in vitro studies employing human cell lines owing to the limited proton energies of <20 MeV available at repetition-rate-capable laser sources[20–23]. Recently, however, emerging petawatt (PW)-class lasers with repetition rates at the hertz level allow to generate proton bunches at kinetic energies beyond 60 MeV (refs. [24,25]). The penetration capability of these bunches now, in principle, enables dose delivery to three-dimensional samples of millimetre-to-centimetre scale and opens the path to in vivo small animal studies. Yet, advancing a laser–plasma research setup to the performance, instrumentation, readiness and stability level required for high-level interdisciplinary irradiation studies, particularly on living samples, poses a major hurdle to be cleared for LPA sources[26]. As the first step, proof-of-principle irradiation experiments on volumetric samples have recently demonstrated the general applicability of laser-driven proton sources[27,28], showcasing beam delivery solutions adapted to the angular and spectral characteristics of the source[18,27–31]. However, before contributions to radiobiological research can be made, a full proton LPA research platform for small animal studies has to be established. Its realization requires the following:

1. Model-compliant dose delivery: the delivery of variable prescribed homogeneous volumetric dose distributions within the percent-level margins determined by radiobiological protocols, mitigating LPA-inherent spectral intensity fluctuations correlated with variations in the laser or target parameters
2. Accelerator readiness and stability: stable daily accelerator performance over weeks, benchmarked via machine parameters defined by the intended application, as a precondition for beam availability following a schedule determined by in vivo sample preparation
3. Radiobiological pilot study: the emulation of a full-scale radiobiological study at a reduced number of samples benchmarked via meaningful dose–effect data, showcasing the concerted operation of on-demand proton LPA-source operation, precise dose delivery and dosimetry, together with complex in vivo sample preparation, irradiation and follow up

Here we present an experiment that demonstrates the fulfilment of the above requirements in the first successfully conducted small animal pilot study at a proton LPA research platform. The study comprises reference irradiations at a clinical proton source[32] and control animals to exclude irradiation-independent factors in a multifacility experiment[33]. The observed radiation-induced tumour growth delay in a mouse model (sample size, 92 animals), examined at a single-dose point ((4.0 ± 0.4) Gy), proves the achievement of the unique interplay of long-term stable proton LPA-source operation at the highest performance and precise dose delivery and dosimetry adapted to the ultrahigh bunch dose rate at millimetre-scale irradiation fields with the complex requirements of a radiobiological study.

Model-compliant dose delivery

The small animal model used in this work is based on spherical tumours with diameters of ~3 mm superficially grown on a mouse ear. It was developed for radiobiological studies with radiation modalities that allow only small penetration depths[34,35]. A cylindrical planning target volume (PTV) was defined for dose application with 5 mm diameter and 4 mm depth (water equivalent) to account for tumour-shape variation and positioning inaccuracy, whereas the thinness of the mouse ear (~250 µm) keeps the irradiated healthy tissue volume small. To induce an observable tumour growth delay in accordance with the radiobiological model, a PTV dose of $D_{PTV}=(4.0\pm0.4)$ Gy was prescribed. A lower limit of 1 Gy min^{-1} is radiobiologically mandated for the mean dose rate, effectively limiting the overall irradiation time

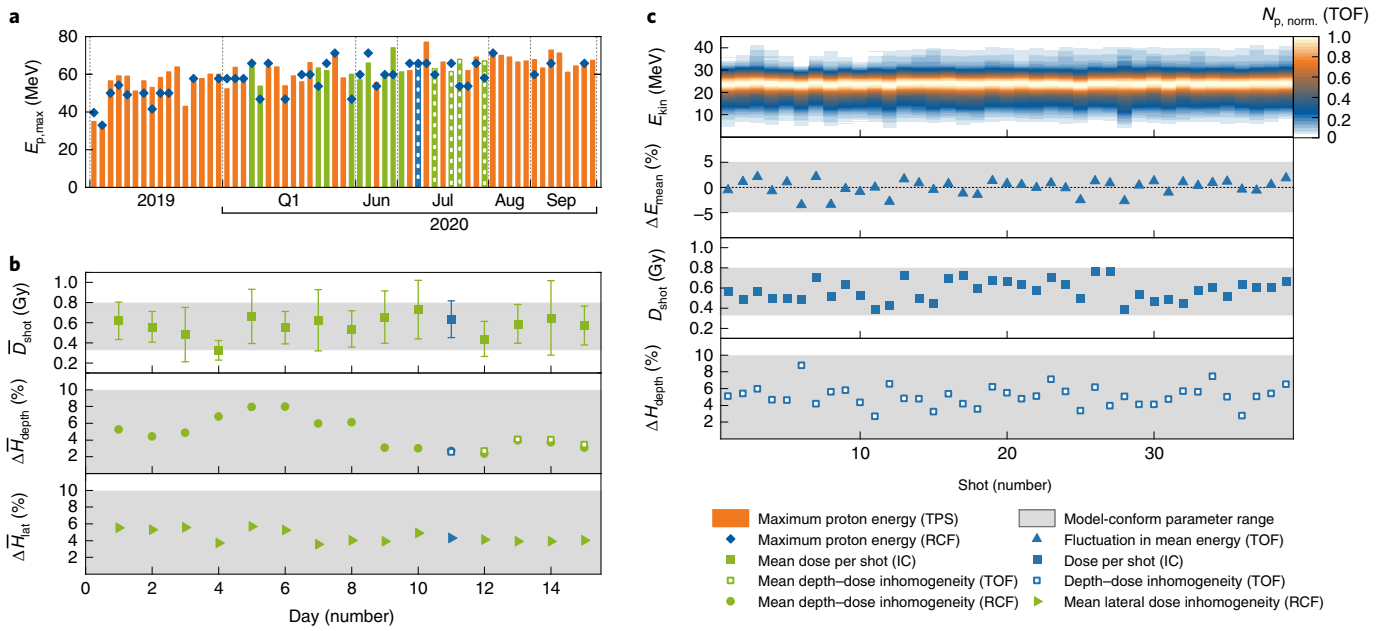

Fig. 2 | Accelerator readiness and beam delivery stability. a, Daily LPA-source performance over a two-year period demonstrated via the highest recorded proton cut-off energy $E_{p,max}$ from the Thomson parabola spectrometer (TPS, bars) and RCF stack (diamonds); the horizontal line at $E_{p,max}=60$ MeV acts as a guide for the eye. The green bars correspond to the data in b and the blue bar, the data in c. Small animal irradiation days are highlighted by the dashed bars. **b**, Daily average of the dose delivery parameters (mean dose per shot $\bar{D}_{shot}$ with 2σ standard deviation, mean depth $\Delta\bar{H}_{depth}$ and lateral dose inhomogeneity $\Delta\bar{H}_{lat}$) and targeted parameter ranges (grey). The blue data points correspond to the data in c. **c**, Verification of the stability of all (consecutive) shots during a representative day of mouse irradiation measured by the transported kinetic-energy spectrum E_{kin} with $N_{p,norm}$ as normalized proton number, relative mean bunch energy fluctuation ΔE_{mean} and dose delivery parameters (dose per shot D_{shot} and depth–dose inhomogeneity per shot ΔH_{depth}), all lying within the targeted parameter ranges (grey).

to 4 min. An inhomogeneity threshold of 10% (2σ) applies to the lateral and depth–dose homogeneity over the entire PTV. The generation of the prescribed depth–dose homogeneity requires a proton distribution that has the spectral shape of a broad, asymmetric triangle. With a peak at around 25 MeV, it provides the necessary penetration depth, whereas its flatter slope towards lower energies contributes a dose to shallower depths, transforming the otherwise pristine to a homogeneous spread-out Bragg peak[29]. In total, ~10^8 particles are needed to meet the prescribed dose over the 80 mm^3 PTV considering a mean proton energy of 20 MeV. The requirements pose major challenges for a laser-driven dose delivery system, comprising primary source optimization, beam tailoring and dedicated diagnostics for guidance and monitoring. Yet, overcoming these challenges opens up unique possibilities for single-shot tumour-conform irradiation.

Irradiation with LPA protons was performed at the Draco PW laser at Helmholtz-Zentrum Dresden-Rossendorf[36]. Draco PW delivered up to 18 J in 30 fs on the target. Protons are emitted from plastic foils of ~220 nm thickness, exhibiting the exponentially decaying LPA energy spectrum with a well-defined cut-off energy of up to ~70 MeV. The spectrum yields enough particles within the crucial energy window between 15 and 40 MeV (Fig. 1b, black curve) to perform single-shot dose delivery[25]. The source spectrum was adapted to the PTV specifications using a pulsed two-solenoid beamline with inherent chromatic energy transfer function and high transport efficiency in combination with apertures and scatterers, allowing for the active shaping of various three-dimensional dose profiles in a single shot[27]. To monitor the proton beam in the irradiation volume and guide the beam-transport tailoring process, a transmissive scintillator-based time-of-flight (TOF) spectrometer was developed. It provides the proton spectrum for the entire PTV and hence a calibrated on-shot depth–dose profile prediction (Fig. 1b,c and Methods).

We optimize the beamline to transport a broad-energetic proton bunch and subsequently fine-tune its spectral shape via the energy selection aperture (ESA) between the solenoids to enable single-shot depth–dose homogenization. This technique exploits the energy-dependent beam size at the ESA position, where protons of higher energies have larger beam diameters because of the rising focal length of the solenoid lens with increasing particle energy. Reducing the size of the ESA decreases the transport efficiency on the high-energy side of the spectrum, which leads to a relative elevation of the low-energy pedestal, thus approaching the required triangular spectral shape (Fig. 1c). The accumulated depth–dose profile (Fig. 1d) demonstrates the procedure's capability of depth–dose homogenization. Lateral beam confinement and homogeneity are achieved with the final beam aperture and scatterers downstream of the second solenoid.

For the prescribed dose delivery within the model-defined percent-level margins, we applied a multishot irradiation scheme with a defined single-shot dose range of 330–800 mGy. The lower limit is given by the applicable repetition rate of the pulsed solenoids (up to three shots per min) together with the mandatory mean dose rate of 1 Gy min^{-1} (preventing an otherwise reduced dose response[37]). The upper limit is set by the specified accuracy of the prescribed dose value of 4 Gy, demanding the accumulation of at least five shots accounting for shot-to-shot dose fluctuations (up to ±20%). The adjustment of the single-shot dose was realized by reducing the laser input energy that tailors the proton yield at negligible spectral changes within the relevant energy bandwidth (Fig. 1b, orange and black spectra). A calibrated transmission ionization chamber (IC), installed behind the TOF spectrometer, is used to monitor the single-shot dose as well as terminate the irradiation when the prescribed dose window is reached. During mouse irradiation, a single dosimetry radiochromic film (dRCF) is placed in front of the tumour to verify the accumulated dose value and lateral dose

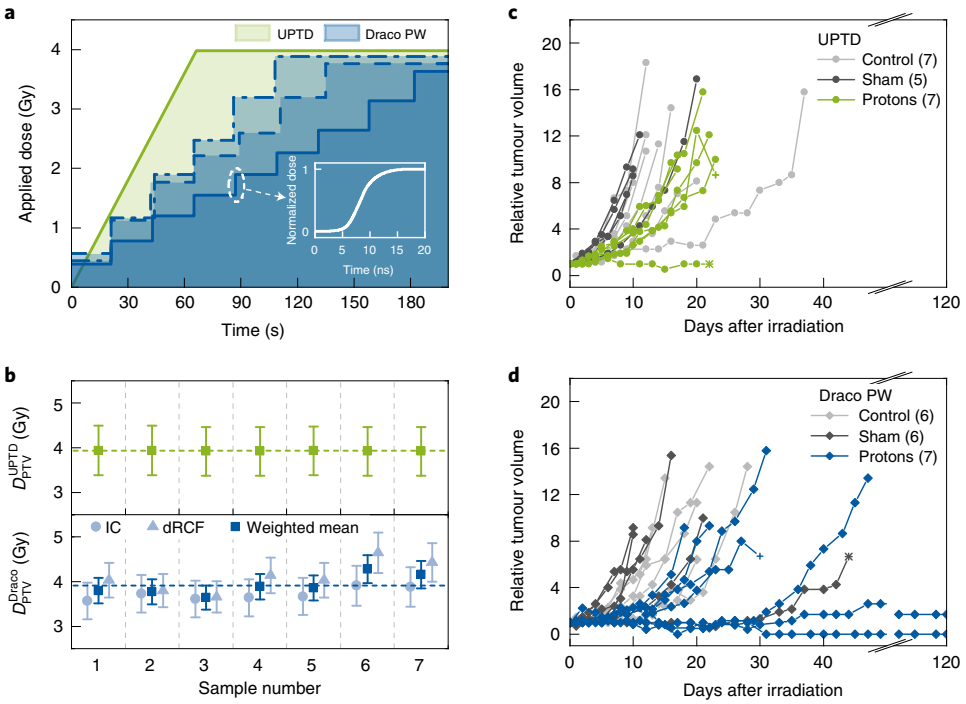

Fig. 3 | Radiobiological pilot study and follow up (reference proton data (cyclotron at UPTD) in green; LPA proton data (Draco PW) in blue). a, Examples of irradiation timescales; the continuous irradiation of the UPTD cyclotron is indicated in green and pulsed irradiation of three selected mice at Draco PW, in blue. The inset shows a rapid dose application by the LPA proton bunch. **b**, Proton tumour doses of all the mice including 2σ uncertainties at the cyclotron ($D_{\mathrm{PTV}}^{\mathrm{UPTD}}$) and laser accelerator ($D_{\mathrm{PTV}}^{\mathrm{Draco}}$). The final dose values at Draco PW as the weighted mean of two independent absolute dosimetry methods (IC and dRCF; light blue). The mean values for all the animals are given by dashed lines. **c**,**d**, Individual tumour growth curves as the relative tumour volume increases after allocation/treatment for growth control (light grey), sham (dark grey) and proton-irradiated (green/blue) mice at the respective facilities. Tumour growth of the sham-treated groups, which run in parallel to the irradiated ones, indicate the influence of the respective treatment conditions. Unaffected tumour growth is shown by the control mice that remain in the corresponding animal facilities. The asterisks indicate mice with fast-growing secondary tumours, and the plus signs indicates tumour volume reduction due to scabbing. The number of animals per group is given in the parentheses. The *x* axis is interrupted to display a longer period of time with no substantial change in tumour volume.

profile, whereas the depth–dose homogeneity is monitored with the TOF spectrometer for every shot. Figure 1d shows an example of the depth–dose data (orange histogram) and selected images of the lateral dose distribution (false colour) of one RCF stack irradiated for quality assurance (QA). The prediction of the TOF spectrometer perfectly matches the RCF-measured depth–dose profile. The measured dose value of $D_{\mathrm{PTV}} = 4.0$ Gy accumulated over six shots (in 105 s) at a mean dose per shot of 660 mGy meets the model specifications. Both relative lateral (ΔH_{lat}) and depth–dose inhomogeneity ($\Delta H_{\mathrm{depth}}$), evaluated as the 2σ standard deviation of the mean dose within the depicted 5 mm regions of interest of RCF layers 2–12 (striped histogram section) corresponding to the PTV, are well within the 10% boundary, with $\Delta H_{\mathrm{lat}} = 5\%$ and $\Delta H_{\mathrm{depth}} = 4\%$. The utilization of the spectrally broad LPA source is demonstrated by comparing the input spectrum (Fig. 1b, orange line) and single-shot TOF spectrum (Fig. 1b, blue line). This TOF spectrum represents all the protons required at the source level for dose delivery to the PTV and therefore was scaled accounting for particle loss (apertures) and energy shifts (scatterers) during transport. The established research platform enables the delivery of three-dimensional tumour-conform dose distributions in agreement with all the specifications for quantitative in vivo radiobiological experiments by making perfect use of the broadband proton spectrum uniquely available at an LPA source.

Accelerator readiness and stability

Before an animal can be allocated to the experiment, the irradiation setup, beam formation and monitoring methods need to be developed and their functionalities need to be demonstrated. This has been performed by verifying animal-model-defined beam readiness parameters for daily beam availability, long-term reliability and shot-to-shot stability, setting new standards for quality control in proton LPA. These parameters and their comparison with the corresponding acceptance window are given in Fig. 2 for the different timescales of interest. The daily available cut-off energy $E_{\mathrm{p,max}}$—the most common parameter for benchmarking laser-driven proton beams—is plotted over the period of two years (Fig. 2a). Mostly close to ~60 MeV, the primary LPA source reliably provides a comfortable safety margin with respect to the required 40 MeV over the long term. On selected days dedicated for campaign preparation or mouse irradiation itself (Fig. 2a, green and blue bars), ranging over a half-year period, we performed all the procedures from start up to irradiation (QA RCF stacks or mice) to verify the daily availability of application-specific dose delivery parameters. Figure 2b depicts the daily average values (denoted by the overbar) obtained for the dose per shot $\bar{D}_{\mathrm{shot}}$, relative depth–dose inhomogeneity $\Delta\bar{H}_{\mathrm{depth}}$ and relative lateral dose inhomogeneity $\Delta\bar{H}_{\mathrm{lat}}$. Figure 2c summarizes the shot-to-shot stability during a selected day (Fig. 2a,b, blue-coloured data) of the irradiation campaign. The two graphs on top show the considerably high spectral stability of the transported bunches, depicted by the normalized spectral bunch composition determined via TOF, and the corresponding relative fluctuation of the mean bunch energy ΔE_{mean} (Fig. 1c). The fluctuation in the dose per shot D_{shot} depicted below again accentuates the importance of the multishot dose delivery scheme applied. The plot is completed by the depth–dose inhomogeneity score $\Delta H_{\mathrm{depth}}$ deduced from the TOF spectrum.

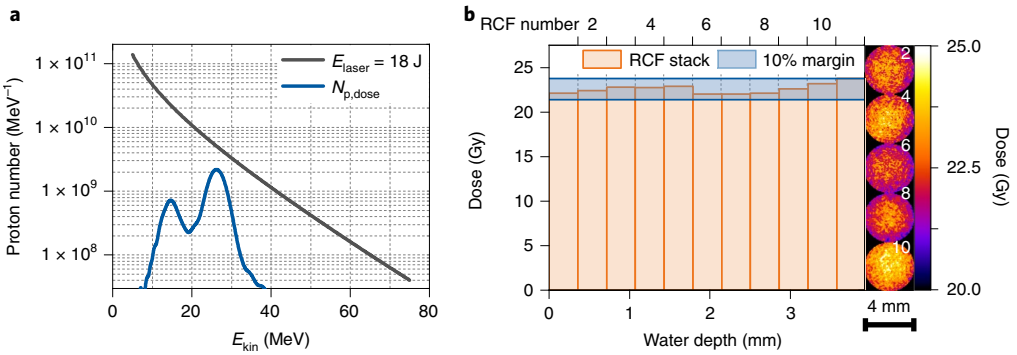

Fig. 4 | Single-shot ultrahigh-dose-rate capability (cf. Fig. 1b,d). a, RCF-measured kinetic energy (E_{kin}) proton-source spectrum at the maximum laser energy E_{laser} = 18 J on the target (black) and proton spectrum, contributing to the delivery of a single-shot dose of 22.6 Gy (mean of the depth–dose distribution measured via the RCF stack) after shot-dose-optimized transport ($N_{p,dose}$; blue). The data are taken at Draco PW (Methods). **b**, Respective depth–dose profile with a homogeneity margin of 10% (blue). Exemplary pseudo-colour images show lateral dose distributions at selected RCF stack layers within the PTV.

Simultaneously meeting all the prescribed parameter ranges (Fig. 2, grey bars) represents a breakthrough in every aspect: the demonstration of laser-driven proton-beam generation at this high-energy level over two years, dose delivery at radiobiologically relevant quality and high-precision dosimetry over many weeks and for every shot of each required day.

Radiobiological pilot study

In preparation of the irradiation experiments, human head and neck squamous cell carcinoma tumour cells (~10^5) were injected into the mouse ears to induce tumour growth[35]. Animals bearing tumours were allocated for treatment when a single tumour with a diameter of about 3 mm had developed. The tumour on the ear of the anaesthetized mouse was then precisely aligned at the irradiation position (Fig. 1a, right) for the application of the prescribed single-dose point of (4.0 ± 0.4) Gy. After irradiation, the tumour growth was followed up over a period of up to 120 days to reveal treatment-dependent differences. As a reference to the experiment at the LPA source, a subsequent experiment on a second cohort of mice was conducted at the University Proton Therapy Dresden (UPTD) (three weeks later) at the campus of the University Hospital Carl Gustav Carus, Dresden. The animals were irradiated at the same dose level as Draco PW by the continuous proton beam of the fixed horizontal research beamline employing a clinically used isochronous cyclotron (C235, IBA)[32]. The irradiation procedure, dosimetry protocol and animal preparation were identical at both facilities. The irradiation of dedicated treatment groups with standard 200 kV X-rays was performed in parallel to each proton experiment to allow the comparison of the radiobiological outcome of the consecutive campaigns and to identify possible deviations in the biological response arising from biological diversity[33]. A total of 61 out of 92 animals were allocated to the experiment. They were divided into two cohorts for the different irradiation sites, and each cohort was divided into five treatment groups (number of animals in Draco PW/number of animals in UPTD): proton irradiated (8/7), proton sham (6/5), X-ray irradiated (5/7), X-ray sham (4/6) and growth control (6/7). The sham-treated groups were identically treated to the irradiation groups, except irradiation. In combination with the control groups that remained in the housing facility without treatment, the sham-treated groups are used to uncover influences of the experimental procedures on tumour growth that are not induced by radiation.

Figure 3a illustrates the temporal dose application at both facilities with comparable mean dose rates of 3.6 Gy min^{-1} for the continuous beam of the cyclotron and 1.2–2.2 Gy min^{-1} for the multishot delivery scheme at the LPA source. The inset shows the rapid dose application on the nanosecond scale for the laser-driven bunches, resulting in peak dose rates of up to 10^8 Gy s^{-1}. Figure 3b summarizes the applied proton tumour dose values, evaluated over the PTV, including dosimetric uncertainty in both experiment branches. At UPTD, reproducible dose delivery with an average dose of $D_{PTV}^{UPTD} = 3.9$ Gy (green, Fig. 3b) was applied to the tumours. The average dose for the Draco PW irradiation amounts to $D_{PTV}^{Draco} = 3.9$ Gy (blue, Fig. 3b), whereas all the individual dose values remained within the prescribed dose window. Relative dose uncertainties (2σ) were 14% at UPTD and 8% at Draco PW owing to the two employed dosimetry methods based on independent absolute dosimeters (IC and dRCF). Both dosimetry methods agree well (Fig. 3b, light-blue-coloured data). Dose inhomogeneity was also comparable at both facilities, with a relative lateral inhomogeneity of 9% at UPTD and 6–9% at Draco PW. The relative depth inhomogeneity amounted to 2% at the cyclotron and ranged from 4% to 9% at the laser accelerator. The perfect agreement of the applied dose within all the uncertainty boundaries complies with the strict requirements imposed by the in vivo tumour model and only therefore permits a comparison of the biological data.

Tumour growth data obtained for the mice irradiated with the continuous cyclotron reference and LPA proton beam are shown in Fig. 3c,d. By comparison with the corresponding curves for growth controls and sham irradiations, a clear radiation-induced effect is indicated. A strongly delayed onset of tumour growth or even tumour control—the latter being outside the model framework—was reached for a small number of animals. Although such cases statistically occur, at most, once per treatment group (whether irradiated or not), they accumulate in three out of seven cases in the LPA proton group. This observation motivates further investigations to quantify the efficacy of LPA proton irradiation on the tumour growth at a high statistical significance. Considering the limited sample size of the pilot study, a renormalization of the growth curves in Fig. 3c,d in accordance with the collected X-ray data (Extended Data Fig. 1) was not performed. Yet, X-ray irradiation remains essential in a full-scale study to identify and correct for deviations in the biological response arising from biological diversity between the mouse cohorts at both facilities. In the pilot study at hand, conducted at a cyclotron and an LPA source, no indications for influences of environmental conditions and experimental procedures were found, which is an important precondition for all future studies. Following biostatistical considerations, a total of 22 analysed animals per group are required to detect a disparity of

the radiobiological effect of laser-driven and conventional protons with a level of significance of $\alpha = 0.05$ and a power of 80% assuming a difference of four days in the tumour growth delay. Accounting for a certain safety margin (~30%), a full-scale experiment would comprise a total of almost 300 mice.

A platform for translational research with LPA protons

With the presented in vivo pilot study fulfilling all the requirements in terms of accelerator readiness, delivery of a three-dimensional tumour-conform prescribed dose, dosimetry and radiobiological protocol, we have shown the successful establishment of a proton LPA research platform for small animal studies. This sets new standards for proton LPA sources and paves the way for any subsequent study with this kind of radiation modality across interdisciplinary research fields. Looking beyond the scope of the pilot study, the versatile platform is capable of delivering tailored dose distributions, including RT-relevant spread-out Bragg peaks, to a wide range of irradiation samples featuring a maximum penetration of 40 mm (water equivalent) for 70 MeV protons. At the current highest performance of Draco PW, the efficient transport of broad parts of the LPA proton-source spectrum allows single-shot doses exceeding 20 Gy, homogeneously distributed over millimetre-scale volumes (Fig. 4). During single-shot sample irradiation, the total proton dose would be delivered within ~10 ns, resulting in identical mean and bunch dose rates of 10^9 Gy s^{-1}. Electron-bunch dose rates of a similar order have induced a FLASH effect in zebrafish embryos[38]. Verifying this behaviour with protons is a promising near-future application for such a short-pulse, ultrahigh-dose-rate proton source. Further applications include the investigation of radiochemistry in the context of FLASH[39,40] and the continuation of preclinical cell and small animal studies for a better understanding of basic mechanisms and requirements.

The achievement of the previously inaccessible combination of dose delivery parameters in this study and the demonstrated ability to provide radiobiological data comparable to a clinical reference show that LPA research facilities not only extend the portfolio of proton sources for translational research in general but also carry the potential to contribute to proton FLASH RT research.

Online content

Any methods, additional references, Nature Research reporting summaries, source data, extended data, supplementary information, acknowledgements, peer review information; details of author contributions and competing interests; and statements of data and code availability are available at https://doi.org/10.1038/s41567-022-01520-3.

Received: 11 August 2021; Accepted: 21 January 2022;
Published online: 14 March 2022

References

1. Baumann, M. et al. Radiation oncology in the era of precision medicine. *Nat. Rev. Cancer* **16**, 234–249 (2016).
2. Baumann, M. et al. The translational research chain: is it delivering the goods? *Int. J. Radiat. Oncol. Biol. Phys.* **49**, 345–351 (2001).
3. Favaudon, V. et al. Ultrahigh dose-rate FLASH irradiation increases the differential response between normal and tumor tissue in mice. *Sci. Transl. Med.* **6**, 245ra93 (2014).
4. Bourhis, J. et al. Clinical translation of FLASH radiotherapy: why and how? *Radiother. Oncol.* **139**, 11–17 (2019).
5. Vozenin, M.-C. et al. Biological benefits of ultra-high dose rate FLASH radiotherapy: sleeping beauty awoken. *Clin. Oncol.* **31**, 407–415 (2019).
6. Wilson, J. D. et al. Ultra-high dose rate (FLASH) radiotherapy: silver bullet or fool's gold? *Front. Oncol.* **9**, 1563 (2020).
7. Diffenderfer, E. S. et al. The current status of preclinical proton FLASH radiation and future directions. *Med. Phys.* https://doi.org/10.1002/mp.15276 (2021).
8. Ruan, J.-L. et al. Irradiation at ultra-high (FLASH) dose rates reduces acute normal tissue toxicity in the mouse gastrointestinal system. *Int. J. Radiat. Oncol. Biol. Phys.* **111**, 1250–1261 (2021).
9. Montay-Gruel, P. et al. Hypo-fractionated FLASH-RT as an effective treatment against glioblastoma that reduces neurocognitive side effects in mice. *Clin. Cancer Res.* **27**, 775–784 (2020).
10. Vozenin, M.-C. et al. All irradiations that are ultra-high dose rate may not be FLASH: the critical importance of beam parameter characterization and in vivo validation of the FLASH effect. *Radiat. Res.* **194**, 571–572 (2020).
11. Esplen, N. et al. Physics and biology of ultrahigh dose-rate (FLASH) radiotherapy: a topical review. *Phys. Med. Biol.* **65**, 23TR03 (2020).
12. Hughes, J. R. & Parsons, J. L. FLASH radiotherapy: current knowledge and future insights using proton-beam therapy. *Int. J. Mol. Sci.* **21**, 6492 (2020).
13. Beyreuther, E. et al. Feasibility of proton FLASH effect tested by zebrafish embryo irradiation. *Radiother. Oncol.* **139**, 46–50 (2019).
14. Diffenderfer, E. S. et al. Design, implementation, and in vivo validation of a novel proton FLASH radiation therapy system. *Int. J. Radiat. Oncol. Biol. Phys.* **106**, 440–448 (2020).
15. Jolly, S. et al. Technical challenges for FLASH proton therapy. *Phys. Medica* **78**, 71–82 (2020).
16. Cunningham, S. et al. FLASH proton pencil beam scanning irradiation minimizes radiation-induced leg contracture and skin toxicity in mice. *Cancers* **13**, 1012 (2021).
17. Albert, F. et al. 2020 roadmap on plasma accelerators. *New J. Phys.* **23**, 031101 (2021).
18. Aymar, G. et al. LhARA: the laser-hybrid accelerator for radiobiological applications. *AIP Conf. Proc.* **8**, 567738 (2020).
19. Cirrone, G. A. P. et al. ELIMED-ELIMAIA: the first open user irradiation beamline for laser-plasma-accelerated ion beams. *AIP Conf. Proc.* **8**, 564907 (2020).
20. Yogo, A. et al. Application of laser-accelerated protons to the demonstration of DNA double-strand breaks in human cancer cells. *Appl. Phys. Lett.* **94**, 181502 (2009).
21. Zeil, K. et al. Dose-controlled irradiation of cancer cells with laser-accelerated proton pulses. *Appl. Phys. B* **110**, 437–444 (2013).
22. Hanton, F. et al. DNA DSB repair dynamics following irradiation with laser-driven protons at ultra-high dose rates. *Sci. Rep.* **9**, 4471 (2019).
23. Bayart, E. et al. Fast dose fractionation using ultra-short laser accelerated proton pulses can increase cancer cell mortality, which relies on functional PARP1 protein. *Sci. Rep.* **9**, 10132 (2019).
24. Kim, I. J. et al. Radiation pressure acceleration of protons to 93 MeV with circularly polarized petawatt laser pulses. *Phys. Plasmas* **23**, 070701 (2016).
25. Ziegler, T. et al. Proton beam quality enhancement by spectral phase control of a PW-class laser system. *Sci. Rep.* **11**, 7338 (2021).
26. Chaudhary, P. et al. Radiobiology experiments with ultra-high dose rate laser-driven protons: methodology and state-of-the-art. *Front. Phys.* **9**, 624963 (2021).
27. Brack, F.-E. et al. Spectral and spatial shaping of laser-driven proton beams using a pulsed high-field magnet beamline. *Sci. Rep.* **10**, 9118 (2020).
28. Rösch, T. F. et al. A feasibility study of zebrafish embryo irradiation with laser-accelerated protons. *Rev. Sci. Instrum.* **91**, 063303 (2020).
29. Masood, U. et al. A compact solution for ion beam therapy with laser accelerated protons. *Appl. Phys. B* **117**, 41–52 (2014).
30. Romano, F. et al. The ELIMED transport and dosimetry beamline for laser-driven ion beams. *Nucl. Instrum. Methods Phys. Res. A* **829**, 153–158 (2016).
31. Zhu, J. G. et al. Demonstration of tailored energy deposition in a laser proton accelerator. *Phys. Rev. Accel. Beams* **23**, 121304 (2020).
32. Beyreuther, E. et al. Research facility for radiobiological studies at the University Proton Therapy Dresden. *Int. J. Part. Ther.* **5**, 172–182 (2019).
33. Oppelt, M. et al. Comparison study of in vivo dose response to laser-driven versus conventional electron beam. *Radiat. Environ. Biophys.* **54**, 155–166 (2015).
34. Brüchner, K. et al. Establishment of a small animal tumour model for in vivo studies with low energy laser accelerated particles. *Radiat. Oncol.* **9**, 57 (2014).
35. Beyreuther, E. et al. An optimized small animal tumour model for experimentation with low energy protons. *PLoS One* **12**, e0177428 (2017).
36. Schramm, U. et al. First results with the novel petawatt laser acceleration facility in Dresden. *J. Phys.: Conf. Ser.* **874**, 012028 (2017).
37. Hall, E. J. & Brenner, D. J. The dose-rate effect revisited: radiobiological considerations of importance in radiotherapy. *Int. J. Radiat. Oncol. Biol. Phys.* **21**, 1403–1414 (1991).
38. Pawelke, J. et al. Electron dose rate and oxygen depletion protect zebrafish embryos from radiation damage. *Radiother. Oncol.* **158**, 7–12 (2021).
39. Oulianov, D. A. et al. Ultrafast pulse radiolysis using a terawatt laser wakefield accelerator. *J. Appl. Phys.* **101**, 053102 (2007).
40. Jansen, J. et al. Does FLASH deplete oxygen? Experimental evaluation for photons, protons, and carbon ions. *Med. Phys.* **48**, 3982–3990 (2021).

Methods

Setup at UPTD. The existing double-scattering setup at the fixed horizontal beamline[41] was used to deliver a homogeneous proton field. The proton range, and hence the spread-out Bragg-peak position, was shifted by 90.0 mm poly(methyl methacrylate) (PMMA) (stopping power ratio, 1.18) and 122.4 mm polycarbonate (stopping power ratio, 1.15 (ref. [32])) slabs. The final beam aperture (lead and aluminium; 7 mm diameter) defines the irradiation field.

Setup at Draco PW. Single-plasma-mirror-cleaned laser pulses[25] with energies of ~10 J (reduced-energy shot) to ~18 J (full-energy shot) were focused (2.6 µm full-width at half-maximum) onto 220-nm-thick formvar foils under oblique incidence (50°), leading to intensities on target of 3.0 and 5.4×10^{21} W cm^{-2}, respectively, with a repetition rate of 3–4 shots per minute. Temporal pulse-shape optimization for the highest cut-off energies was conducted according to another study[25] via a Thomson parabola spectrometer (at the end of the beamline) and a proton-beam profiler every day. After optimization of the LPA source, knowing the geometrical and spectral source characteristics in the beam transport direction, the in-air irradiation setup is assembled and the beamline is prepared within 10 min. The overall setup follows the concept presented elsewhere[27], with the following key components and respective distances to the laser target (Fig. 1). Solenoid 1 (magnetic flux density $B_1 \approx 13.6$ T at the solenoid centre, 40 mm bore, first winding at 77 mm), ESA (aluminium; 15 mm diameter, at 745 mm), solenoid 2 ($B_2 = 3.5$ T at the solenoid centre, 42 mm bore, first winding at 1,108 mm), first scatter foil (nickel; 220 µm, at 1,820 mm), Kapton window (75 µm thickness, 30 mm diameter, at 2,005 mm), second scatter foil (nickel; 110 µm, at 2,010 mm), TOF detector and transmission IC (14 mm diameter, at 2,082 mm) and final beam aperture (lead and aluminium; 7 mm diameter, at 2,135 mm). Solenoid 1 was equipped with a dedicated cooling system that allowed continuous operation at three pulses per minute.

Beam transport at Draco PW. The model-assisted beam transport scheme based on another study[27] employs two pulsed solenoid magnets that act as chromatic lenses selectively focusing two spectral components of the broad LPA source at the PTV position for homogeneous depth–dose formation.

For precise accumulative dose delivery, as applied for mouse irradiation, the gap between the transported spectral components was deliberately widened and the lower-energetic part was stopped in the scatterers. Together with the spectral manipulation via ESA (Fig. 1c), this measure aided the adjustment of the dose per shot, complementary to applying low-energy laser shots, and made the depth–dose homogeneity more robust with respect to fluctuations in the LPA source. Single-shot high-dose delivery (Fig. 4) requires peak proton-source intensities, that is, full-energy laser shots, as well as the simultaneous efficient transport of both spectral components superimposed at the PTV for dose escalation and maintaining radiobiological homogeneity constraints (Fig. 4b). The use of apertures and scatterers was therefore kept to a minimum.

The spectral distribution of the transported proton bunch was measured by the TOF spectrometer and compared with the reference spectra. If necessary, beam transport was readjusted by tuning the magnetic-field strength (typical changes of <4%) of the solenoids. The alignment of the (motorized) final beam aperture with respect to the beam axis was performed via online scintillator measurements.

The beam transport setup offers a direct line of sight from the source to the sample, making it necessary to consider the contamination of the transported proton beam at the irradiation site with other ionizing radiation generated in the LPA process or via secondary interaction. Heavier ion species, for example, oxygen or carbon, are transported like protons considering identical magnetic rigidity; however, owing to their low penetration depth, they are stopped by the scatterers and do not contribute to the delivered dose. Electrons are deflected and dispersed in the solenoid fringe fields. The flux of neutral particles at the irradiation site, such as gamma radiation or (secondary) neutrons, is strongly supressed by the ~2 m distance to the source following the inverse-square law. Measurements via RCFs at the irradiation site verified the negligible dose contribution of the radiation background.

Experimental and dosimetric workflow at Draco PW. After optimizing the source and transport, we routinely performed QA measurements before sample irradiation. The QA protocol included the verification of the transmission IC calibration and irradiation of an RCF stack mimicking the radiobiological sample irradiation, including time-critical dose application. The stack was immediately evaluated for delivered dose value and dose homogeneity. When the radiobiological target parameters were not met, we made readjustments at the source level (laser energy) or transport system (magnetic-field strengths, aperture size and so on). Once within the specification, we continued to prepare the radiobiological sample irradiation, during which two independent absolute-calibrated dosimeters are employed. The transmission IC monitors the single-shot dose to terminate the irradiation after reaching the targeted dose window. A single RCF (dRCF), directly in front of the sample, is used for measuring the lateral dose homogeneity. Data for both dosimeters (dRCF and IC), each complemented by TOF measurements, are used to extrapolate their measured dose at the respective detector plane to the averaged dose over the whole sample depth, providing two independent PTV dose values (Fig. 3b, data in light blue). Each sample irradiation was followed by QA RCF stack measurement. The RCFs were digitized in accordance with the calibration protocol.

RCFs. At both facilities, Gafchromic EBT3 films were applied for dose-rate-independent[42] and spatially resolving absolute dosimetry of protons and X-rays for integral doses of ~4 Gy, as applied to the sample. The RCFs were calibrated in homogeneous radiation fields of 200 kV X-rays and spread-out Bragg-peak protons at UPTD as described elsewhere[32]. For dose evaluation, the films were digitized with a flatbed scanner and analysed on the basis of the calibration.

IC. For online dosimetry including the termination of irradiation after the prescribed dose delivery, transmission ICs were used at both facilities (Draco PW, PTW type 7862; UPTD, PTW type 34058) and cross-calibrated against a factory-calibrated Advanced Markus IC (PTW type 34045) at the irradiation site on a daily basis. The Markus IC was read out by a UNIDOS dosimeter (PTW) with air pressure, temperature and radiation-quality corrections applied. Precise dosimetry in ultrahigh-dose-rate proton fields requires special care[43] as saturation effects occur in ICs. A proper saturation correction in accordance with another study[44], verified by complementary RCF measurement, enabled the use of the Markus IC at Draco PW and thus IC cross-calibration. The beam stability of the clinical accelerator at the UPTD enables to deduce the absolute volumetric dose information from the calibrated transmission IC, rendering complementary dosimeters unnecessary, assuming regular accelerator QA.

TOF spectrometer. The TOF spectrometer combines a fast scintillator (200 µm thickness; BC-422Q, Saint-Gobain Crystals) with optical-fibre readout for signal transfer unaffected by the electromagnetic pulse of the LPA process. The signal is digitized by a well-shielded fast photodiode. The temporal resolution of the complete TOF assembly amounts to ~1.5 ns (full-width at half-maximum), calibrated via ultraviolet short-pulse laser excitation. The proton spectrum measured at the TOF position was used to predict the depth–dose distribution at the PTV (Fig. 1d) and reconstruct the proton spectrum at the source that contributes to dose delivery (Fig. 1b). Both calculations were performed via the Monte Carlo code Fluka[45]. Proton-beam size and divergence at multiple positions during transport were measured via the RCF stack and the derived data were fed into the Fluka model. The predicted depth–dose distribution at the PTV was regularly verified via the RCF stack measurement for QA purposes.

Radiobiological protocol. The animal facilities and the experiments were approved according to the European Parliament and Council Directive 2010/63/EU on the protection of animals used for scientific purposes, German animal welfare regulations and local ethics committee (approval DD24-5131/338/35, Saxony State Directorate, Dresden, Germany). The experiments were performed using 7-to-14-week-old female and male NMRI Foxn1$^{(nu/nu)}$ mice purchased from Charles River Laboratories two weeks prior to the tumour injection. The animals were kept grouped with a maximum of eight mice per Euro-standard type III cage at 12:12 h light–dark cycle, constant temperature of about 26 °C and relative humidity of 45–60%. The mice were fed with commercial laboratory animal diet for nude mice and water ad libitum. The optimized mouse ear tumour model[35] was applied using the described procedures for whole-body irradiation, tumour cell preparation and injection, as well as anaesthesia with the exception of introducing Bepanthen eyecream for eye protection during irradiation. Tumour growth was monitored three times a week using a caliper. The corresponding tumour volumes were calculated as $\frac{\pi}{6} \times a \times b^2$, where a is the longest tumour axis and b is the shortest tumour axis perpendicular to a. The tumour origin was routinely controlled by a microsatellite analysis and standard hematoxylin and eosin staining. Tumour-bearing animals fulfilling the allocation criteria[35] were randomly allocated to the different treatment groups necessary to delineate the temporal variances of the tumour model and non-radiation effects from the treatment outcome[33].

For this pilot study, no statistical methods were used to predetermine the sample sizes, but accepted/typical numbers from approved animal studies were applied. Here 92 animals—47 at the laser-driven proton facility Draco PW and 45 at the proton reference facility UPTD—were applied, targeting seven animals per treatment group or 70 animals in total in the analysis, including backup animals to balance for the missing tumour growth, not matching the allocation criteria and exclusion due to health status or radiation failure. Altogether, 61 out of the 92 animals were allocated in both cohorts, whereas 19 animals did not develop a tumour, 11 animals did not meet the allocation criteria and one animal was prematurely euthanized due to general health conditions. One animal was excluded from the analysis after irradiation, because of underdosage at Draco PW due to a technical failure.

Mouse irradiation workflow. A common workflow for mouse irradiation was applied to minimize external influences. Once allocated, the animals were transported to the respective treatment site and anaesthetized shortly before their respective (sham) irradiation. The animals were prone positioned in the prewarmed bedding unit with the tumour-bearing ear fixed with Leukosilk

(BSN Medical) on a PMMA block attached on the right side of the bedding unit. At both proton sources, the bedding unit was set in a holder, where it was tilted by −90° to position the tumour within the radiation field. Camera-based tumour-positioning control assures congruence of the tumour volume and PTV. The final beam aperture assures radiation protection of the mouse. For irradiation with 200 kV X-rays, the bedding units were positioned horizontally superimposing the tumour-bearing ears on the PMMA block with the collimator openings. Independent of the radiation source, the bedding units were heated during irradiation to circumvent a drop in the body temperature of the anaesthetized mice.

Radiobiological follow up and analysis. Following irradiation, tumour diameters were measured blinded three times a week for up to 120 days. The health status was assessed in parallel. The animals were killed by cervical dislocation when the tumour reached the maximum diameter of 7–8 mm, when necessitated by declining animal health status or at the end of the follow-up period. Animals with ulcerated tumours were also excluded. Tumour growth curves (Fig. 3c,d) were derived by relating the measured tumour volumes to the tumour volume at allocation day and treatment start to calculate the relative tumour volume. Tumour growth curves averaged over the respective treatment groups were not calculated due to low statistics. In the X-ray irradiation data (Extended Data Fig. 1), both irradiated treatment groups show a behaviour comparable to their respective growth control and sham irradiation groups. Although the radiation-induced effect might be resolvable in a full-scale study, the data suggest that increasing the applied X-ray dose (compared with the proton dose) in future studies could be beneficial, allowing to more robustly identify potential influences of environmental conditions and experimental procedures at the different irradiation facilities[33].

Reporting Summary. Further information on research design is available in the Nature Research Reporting Summary linked to this article.

Data availability

The source data are available via Rodare at https://doi.org/10.14278/rodare.1128 (ref. [46]). All other data that support the plots within this paper and other findings of this study are available from the corresponding author upon reasonable request.

Code availability

The code written for use in this study is available from the corresponding author upon reasonable request.

References

41. Helmbrecht, S. et al. Design and implementation of a robust and cost-effective double-scattering system at a horizontal proton beamline. *J. Instrum.* **11**, T11001 (2016).
42. Karsch, L. et al. Dose rate dependence for different dosimeters and detectors: TLD, OSL, EBT films, and diamond detectors. *Med. Phys.* **39**, 2447–2455 (2012).
43. Schüller, A. et al. The European Joint Research Project UHDpulse—metrology for advanced radiotherapy using particle beams with ultra-high pulse dose rates. *Phys. Med.* **80**, 134–150 (2020).
44. Gotz, M. et al. A new model for volume recombination in plane-parallel chambers in pulsed fields of high dose-per-pulse. *Phys. Med. Biol.* **62**, 8634–8654 (2017).
45. Böhlen, T. T. et al. The FLUKA code: developments and challenges for high energy and medical applications. *Nucl. Data Sheets* **120**, 211–214 (2014).
46. Kroll, F. et al. Source data repository. *Zenodo* https://doi.org/10.14278/rodare.1128 (2021).

Acknowledgements

We thank T. Hermannsdörfer, S. Zherlitsyn and the workshop of the Dresden High Magnetic Field Laboratory for advice and magnet manufacturing. We acknowledge M. Pfeifer of the Institut of Forensic Medicine (TU Dresden) and W. Eicheler of OncoRay for verification of the tumour model and thank the animal husbandry staff at OncoRay and HZDR. We recognize the support of the Weizmann-Helmholtz Laboratory for Laser Matter Interaction (WHELMI). We are very grateful for the long-lasting support of R. Sauerbrey and W. Enghardt. The work was supported by Laserlab Europe V (PRISES, contract no. 871124). The research infrastructure at the University Proton Therapy Dresden (UPTD) has received funding from the European Union's Horizon 2020 Research and Innovation Programme under grant agreement no. 730983 (INSPIRE).

Author contributions

F.K., F.-E.B., C.B., S.B., E. Bodenstein, L.G., R.G., U.H., K.B., L.K., T.K., S.K., M.K., E.L., U.M., J.M.-N., A.N., J. Pawelke, T.P., M. Reimold, M. Rehwald, H.-P.S., M.E.P.U., T.Z., K.Z. and E. Beyreuther prepared and/or conducted the experiments. K.B., E.L., S.M, J. Pietzsch and E. Beyreuther contributed to animal handling and care. F.K., F.-E.B., L.G., T.K., U.M. and M. Reimold performed the simulations. S.B., R.G., U.H. and T.P. contributed to laser operation and maintenance. F.K., F.-E.B., K.B., E.L., J.M.-N., A.N., M. Reimold and E. Beyreuther analysed the data. F.K., F.-E.B., J.M.-N., K.Z. and E. Beyreuther wrote the manuscript. T.E.C., M.K., J. Pawelke, J. Pietzsch, C.R., U.S., K.Z. and E. Beyreuther supervised the project. All the authors reviewed the manuscript and contributed to discussions.

Funding

Open access funding provided by Helmholtz-Zentrum Dresden - Rossendorf e. V.

Competing interests

The authors declare no competing interests.

Additional information

Extended data is available for this paper at https://doi.org/10.1038/s41567-022-01520-3.

Supplementary information The online version contains supplementary material available at https://doi.org/10.1038/s41567-022-01520-3.

Correspondence and requests for materials should be addressed to Florian Kroll.

Peer review information *Nature Physics* thanks Marie-Catherine Vozenin, Maria-Grazia Andreassi, Leonida Gizzi and the other, anonymous, reviewer(s) for their contribution to the peer review of this work.

Reprints and permissions information is available at www.nature.com/reprints.

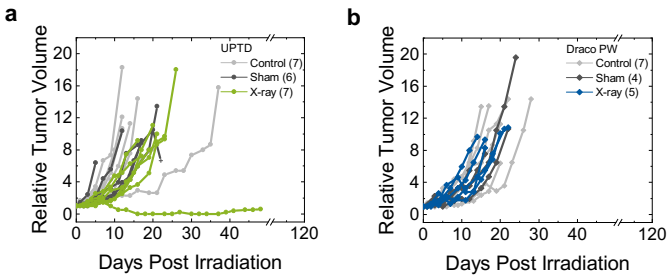

Extended Data Fig. 1 | Individual tumour growth curves as relative tumour volume increase after allocation/treatment. Depicted are growth control (light gray), sham (dark gray) and X-ray irradiated (green/blue) mice at respective facilities: **a** UPTD, **b** Draco PW. Tumour growth of the sham treated groups, which run in parallel to the irradiated ones, indicate the influence of the respective treatment conditions. Unaffected tumour growth is shown by the control mice that remain in the corresponding animal facilities. The plus indicates tumour volume reduction due to scabbing. Number of animals per group given in parentheses. The x-axis is interrupted to display a longer period of time with no substantial tumour volume change.

nature portfolio

Corresponding author(s): Florian Kroll

Last updated by author(s): Feb 15, 2022

Reporting Summary

Nature Portfolio wishes to improve the reproducibility of the work that we publish. This form provides structure for consistency and transparency in reporting. For further information on Nature Portfolio policies, see our Editorial Policies and the Editorial Policy Checklist.

Statistics

For all statistical analyses, confirm that the following items are present in the figure legend, table legend, main text, or Methods section.

n/a	Confirmed	
☐	☒	The exact sample size (*n*) for each experimental group/condition, given as a discrete number and unit of measurement
☐	☒	A statement on whether measurements were taken from distinct samples or whether the same sample was measured repeatedly
☒	☐	The statistical test(s) used AND whether they are one- or two-sided *Only common tests should be described solely by name; describe more complex techniques in the Methods section.*
☒	☐	A description of all covariates tested
☒	☐	A description of any assumptions or corrections, such as tests of normality and adjustment for multiple comparisons
☒	☐	A full description of the statistical parameters including central tendency (e.g. means) or other basic estimates (e.g. regression coefficient) AND variation (e.g. standard deviation) or associated estimates of uncertainty (e.g. confidence intervals)
☒	☐	For null hypothesis testing, the test statistic (e.g. *F*, *t*, *r*) with confidence intervals, effect sizes, degrees of freedom and *P* value noted *Give P values as exact values whenever suitable.*
☒	☐	For Bayesian analysis, information on the choice of priors and Markov chain Monte Carlo settings
☒	☐	For hierarchical and complex designs, identification of the appropriate level for tests and full reporting of outcomes
☒	☐	Estimates of effect sizes (e.g. Cohen's *d*, Pearson's *r*), indicating how they were calculated

Our web collection on statistics for biologists contains articles on many of the points above.

Software and code

Policy information about availability of computer code

Data collection	Python, Excel, camera acquisition tools such as IC Capture
Data analysis	Origin, Excel, Fluka, SRIM, Python, Image J

For manuscripts utilizing custom algorithms or software that are central to the research but not yet described in published literature, software must be made available to editors and reviewers. We strongly encourage code deposition in a community repository (e.g. GitHub). See the Nature Portfolio guidelines for submitting code & software for further information.

Data

Policy information about availability of data

All manuscripts must include a data availability statement. This statement should provide the following information, where applicable:

- Accession codes, unique identifiers, or web links for publicly available datasets
- A description of any restrictions on data availability
- For clinical datasets or third party data, please ensure that the statement adheres to our policy

Source data available from DOI: 10.14278/rodare.1128

Field-specific reporting

Please select the one below that is the best fit for your research. If you are not sure, read the appropriate sections before making your selection.

☒ Life sciences ☐ Behavioural & social sciences ☐ Ecological, evolutionary & environmental sciences

For a reference copy of the document with all sections, see nature.com/documents/nr-reporting-summary-flat.pdf

Life sciences study design

All studies must disclose on these points even when the disclosure is negative.

Sample size	For this pilot study, the aim was to have 7 animals per group in analysis. In order to achieve this goal, backup animals were injected with tumor cells serving as reserve for animals that could not be allocated (no tumor growth) or dropped out after the experiment, e.g., for health reasons or secondary tumor growth. Altogether, 92 animals were applied in this experiment split in 70 animals scheduled for the 10 treatment groups and 22 as backup.
Data exclusions	Tumor growth data from all allocated animals is shown, except one animal that has to be excluded due to an underdosage at the laser-driven proton source (described in manuscript). Altogether, 61 of 92 animals were allocated in both cohorts, whereas 19 animals did not develop a tumor, 11 animals did not meet allocation criteria and 1 animal was prematurely euthanized due to general health conditions.
Replication	The findings could not be replicated since the animal application implies 92 animals for this pilot study. A replication is only feasible within a new animal application.
Randomization	At each experiment day animals whose tumors match the allocation criteria were allocated filling all groups at the respective site in parallel. With this method we want to avoid temporal staggering of fast or slow growing tumor in one group, e.g., by filling the groups one after each other.
Blinding	For allocation, blinding was not possible since the groups were filled in parallel and the animals have to be treated differently in each group. During follow up, the tumor growth was measured as blinded as possible, e.g., by separating animal allocation list and tumor growth data or tumor volume measurements by animal caretakers that were not involved into allocation and treatment.

Reporting for specific materials, systems and methods

We require information from authors about some types of materials, experimental systems and methods used in many studies. Here, indicate whether each material, system or method listed is relevant to your study. If you are not sure if a list item applies to your research, read the appropriate section before selecting a response.

Materials & experimental systems

n/a	Involved in the study
☒	☐ Antibodies
☐	☒ Eukaryotic cell lines
☒	☐ Palaeontology and archaeology
☐	☒ Animals and other organisms
☒	☐ Human research participants
☒	☐ Clinical data
☒	☐ Dual use research of concern

Methods

n/a	Involved in the study
☒	☐ ChIP-seq
☒	☐ Flow cytometry
☒	☐ MRI-based neuroimaging

Eukaryotic cell lines

Policy information about cell lines

Cell line source(s)	FaDu_DD was derived from our own stock.
Authentication	Tumor origin was routinely checked by microsatellite analysis of tumors that could not be allocated. In addition, tumor origin was verified by an in-house expert on basis of hematoxilin and eosin stained slices.
Mycoplasma contamination	We confirmed that the cell line was free of mycoplasma contamination.
Commonly misidentified lines (See ICLAC register)	n/a

Animals and other organisms

Policy information about studies involving animals; ARRIVE guidelines recommended for reporting animal research

Laboratory animals	NMRI nu/nu, male and female, 7-14 weeks purchased from Charles River Laboratories (Sulzfeld, Germany)
Wild animals	The study did not involve wild animals.
Field-collected samples	The study did not involve samples collected from the field.
Ethics oversight	Approval DD24-5131/338/35, Saxony State Directorate, Dresden, Germany

Note that full information on the approval of the study protocol must also be provided in the manuscript.